Integration of ground-based hyperspectral and lidar scanning in virtual outcrop geology

Tobias H. Kurz

Dissertation for the degree philosophiae doctor (PhD)
at the University of Bergen

2011

Dissertation date: 28. January 2011

Integration of ground-based hyperspectral and lidar scanning in virtual outcrop geology

Tobias H. Kurz

Dissertation of the degree philosophiae doctor (PhD)

Uni Research

Centre for Integrated Petroleum Research

University of Bergen

Department of Earth Science

Abstract

The potential to visualize and analyse geological outcrops in a 3D environment has made terrestrial laser scanning (TLS) a standard method in geological field studies. Lidar models can be integrated with high resolution photographs to generate photo-realistic 3D models, also referred to as virtual outcrop models (VOMs) in geological applications. However, the extraction of mineralogy and geochemical variations from VOMs is limited to the visible light of the photographs and to the single spectral band provided by the laser sensor. Imaging spectrometry applied from airborne and spaceborne platforms is an established method for the regional mapping of mineralogy and lithology, utilising the interaction of solar radiation with the Earth's surface. Many minerals and rocks can be mapped and analysed in a non-contact manner by utilizing their diagnostic absorption properties within the visible and particularly within the infrared spectral range.

The aim of this research is to apply imaging spectrometry with a ground-based instrument to enable mineralogical and lithological analysis of near-vertical outcrop sections. The terms ground-based and close-range are used to indicate a near-horizontal setup, as opposed to the nadir view found in airborne and spaceborne applications. A workflow has been developed to integrate hyperspectral classifications with 3D lidar models, to compliment VOMs with reliable information about the mineralogy and geochemical variations in the outcrop. The workflow includes data acquisition, spectral and photogrammetric processing of the hyperspectral images, data integration and classifying VOMs utilising hyperspectral image products. A newly developed hyperspectral imager designed as a compact and lightweight instrument, and therefore practical for field applications, has been used. The HySpex SWIR-320m sensor operates within the short wave infrared light (SWIR) with a spectral range between 1.3-2.5 μm.

The spectral data were processed with methods primarily developed for airborne and spaceborne applications. All images showed a significant amount of image artefacts, mainly related to the irregular illumination-viewing geometry and bad pixels. While image nonuniformities such as bad pixels are a common problem in pushbroom scanning, other artefacts such as intensity gradients in along-track direction are exacerbated by the close-range scanning and panoramic image geometry. Applying different nonuniformity corrections, image artefacts were minimized but could not be completely removed. For materials with 50% reflectance a signal to noise ratio better than 70:1 was achieved. Atmospheric corrections were performed utilising an Empirical Line correction, based on two reference spectra measured from calibrated

Spectralon panels which were placed in the image scene. Due to a restricted view of the upper hemisphere in close-range scanning, the obtained reflectance values need to be considered as conic-directional reflectance. To separate and remove image noise Maximum Noise Fraction transform was applied. Spectral classification and mapping was performed using different approaches including band ratios, Spectral Angle Mapping, Spectral Feature Fitting and Mixture Tuned Match Filtering. Based on a cylindrical camera model, VOMs could be integrated and textured with hyperspectral image products with an accuracy of one image pixel.

Two case studies from different geological settings were carried out, to demonstrate how close-range hyperspectral imaging can help improve the analysis of vertical outcrops. In the Pozalagua quarry (Spain), hydrothermal dolomitized limestone of Cretaceous platform-slope carbonates have been spectrally mapped. Despite very similar chemical and spectral properties, different dolomite and limestone types, as well as calcite could be distinguished and mapped in the outcrop. Spectral differences of two main dolomite types could be related to different manganese and iron contents, as confirmed by chemical analysis. Although detailed spectral analysis was disturbed by surface weathering products, dolomite and limestone were also mapped on weathered surfaces. A limestone unit initially missed by conventional field observations, due to similar visual appearance compared to the surrounding carbonates, was clearly identified and mapped by spectral means. The second field area was Garley canyon (Utah, USA), where a shallow marine, shoreface succession was studied. Carbonate and clay abundances were determined to map and quantify carbonate concretions, and to map siltstone and sandstone in the outcrop. Carbonate concretions have implications for reducing porosity and permeability in shallow marine sandstones.

Results show that close-range imaging spectrometry can provide reliable qualitative and quantitative information about the mineral-chemical composition of exposed surfaces. Further research is required to improve the nonuniformity, atmospheric and topographic correction of the spectral images and to adjust the processing to the close-range scanning and image geometry. However, the method can be adapted to other applications in which the collection and analysis of chemical surface composition and geometric information is required, such as in mining, building damage assessment or in forestry for canopy analysis. With an increased availability of lightweight hyperspectral imagers it is expected that close-range imaging spectrometry will become a sub-discipline in remote sensing, and a standard method in field-based geoscience studies.

Acknowledgements

My sincere gratitude goes to a number of people who have contributed advice, provided support for this project and encouraged and supported me to keep going. First of all, I want to thank my supervisors Simon Buckley and John Howell for giving me the opportunity to do this project, for inspiring and fruitful discussions, sharing time and knowledge with me and also for the quite time consuming manuscript reviewing. It was a pleasure, to work in a social and productive working group. Beside the work, I also remember with joy a number of shared tours or social events either in Bergen or during conferences and fieldwork.

I like to thank Walter Wheeler who contributed general ideas for this project. Chris Clark provided accommodation at his cottage during the fieldwork in Derbyshire, which also allowed John and Simon to celebrate a proper Bonfire Night. Peter Gutteridge guided us to local outcrops in the Peak District and helped us to find the Manystone quarry as suitable scanning test site. My sincere thanks to both. Trond Løke and Ivar Baarstad from Norsk Elektro Optikk A/S are thanked for the introduction to scanner handling and technical support. I also want to thank Rudy Swennen, Julie Dewit, Dave Hunt, and John Thurmond for pleasurable cooperation, for a number of very helpful and inspiring discussions and for the opportunity to implement hyperspectral imaging in the field campaign at the Pozalagua quarry. Thanks also to Danilo Schneider for encouraging discussions regard photogrammetric issues. Ole Meyer is thanked for his technical support to prepare the scanning equipment for fieldwork. Thanks to Martina Suppersberger and Mareile Andersson, who briefed me in sample preparation, and for providing support in laboratory work. Ole Tumyr is thanked for the XRF analysis.

Furthermore, this work would not have been possible without substantial funding, and I therefore acknowledge the Norwegian Research Council, the Centre for Integrated Petroleum Research and Statoil ASA for financial support. CIPR are also thanked for a social and pleasant working environment.

My fellow students and colleagues at CIPR are thanked for a number of social events. Special thanks goes to my friends, my working group, and officemates Christian, Håvard, Tor, Eivind, Andreas, Ola, Nicole, Siri, and Christian for reams of coffee and sofa breaks and relaxing Friday beers. Finally my heartfelt thank goes indeed to my parents and my brothers Matthias and Daniel who at all times gave me the highest support and encouragement.

Contents

Preface

This dissertation, which has been submitted for the degree philosophiae doctor (PhD), is the result of research conducted at the Centre for Integrated Petroleum Research (CIPR) and the Department of Earth Science at the University of Bergen, Norway. The research was carried out within a three-year scholarship as a part of the Virtual Outcrop Geology (VOG) project at CIPR, with additional support from the "Paleokarst in Reservoirs" project.

The VOG project was established to develop and utilise novel quantitative, digital data collection techniques for geological outcrop studies, applicable to analogue studies of hydrocarbon reservoirs and aquifers. Terrestrial laser scanning (TLS), also known as lidar, has become a standard technique to capture the geometry of geological outcrops efficiently and with a high accuracy. However, the identification and the mapping of mineralogy from the lidar data are limited. This research develops a workflow to apply close-range hyperspectral imaging. The hyperspectral imagery is integrated with terrestrial lidar models to ultimately improve the mapping and quantitative analysis of the mineralogy in geological outcrop studies. A recently developed hyperspectral imager is used which is practicable for field applications. This cross-discipline research includes spectral analysis, image processing and geological outcrop mapping and interpretation as well as 3D modelling and photogrammetric processing.

List of publications

Paper 1

Close-range hyperspectral imaging and lidar scanning for geological outcrop analysis:Workflow and methods.

Kurz, Tobias H., Buckley, Simon J., and Howell, John A.

Prepared for submittal to the International Journal of Remote Sensing

Paper 2

Integration of panoramic hyperspectral imaging with terrestrial lidar data.

Kurz, Tobias H., Buckley, Simon J., Howell, John A. and Schneider, Danilo

Submitted to The Photogrammetric Record

Paper 3

Remote lithological mapping of geological outcrops using close range hyperspectral imaging.

Kurz, Tobias H., Buckley, Simon J., and Howell, John A.

Submitted to the Journal of the Geological Society, London

Paper 4

Hyperspectral image analysis of different carbonate lithologies (limestone, karst, hydrothermal dolomites): the Pozalagua Quarry case study (Cantabria, NW Spain).

Kurz, Tobias H., Devit, Julie, Buckley, Simon J., Thurmond, John B., Hunt, David W. and Swennen, Rudy

Accepted by Sedimentology (Note: main revisions are incorporated, but final text editing was not completed prior to submission of this thesis)

Structure of the thesis

This thesis is structured as a "cumulative work" in which the bulk of the research has been authored as scientific articles for peer-reviewed international journals. The **introductory section** outlines the motivation of the research and provides an introduction into the physical concepts of imaging spectrometry and lidar scanning. This part also includes the presentation of the instrumentation. Subsequently, the four scientific articles are presented as separate and complementary parts. Since the research articles have been written as stand-alone journal publications, a small amount of overlapping and repetition appears between the main sections. **Paper 1** introduces ground-based hyperspectral imaging and describes the workflow to apply ground-based hyperspectral and lidar scanning for geological outcrop studies with a focus on the spectral image processing. **Paper 2** assesses the photogrammetric model required to precisely integrate the spectral images and lidar scans, and investigates the photogrammetric performance of this data fusion for geological applications. In

Paper 3, two case studies are used, one in carbonates and the second in siliciclastic sediments, to illustrate the potential of ground-based hyperspectral imaging for geological outcrop studies. In **Paper 4** ground-based hyperspectral imaging is applied to the Pozalagua quarry (Spain), to map and quantify different mineral fabrics and other sedimentary products in a carbonate environment. The **concluding section** discusses the main results of the study and gives an outlook for further required research.

Authorship statement

As required by the regulations for cumulative PhD theses at the University of Bergen, the following authorship statement is given to specify the author contributions for each journal paper. I am the first author of the four presented papers, and responsible for the bulk of the research. The data were collected together with Simon Buckley and John Howell; I was responsible for the hyperspectral data and Simon Buckley for the lidar data.

- **Paper 1:** Kurz, Tobias H., Buckley, Simon J., and Howell, John A.: **Close-range hyperspectral imaging and lidar scanning for geological outcrop analysis: Workflow and methods.** *Prepared for submittal to the International Journal of Remote Sensing*

I am responsible for the processing, analysis and interpretation of the hyperspectral data, establishing the complete workflow and for preparing and writing the manuscript. The lidar data were processed by Simon Buckley. The data integration was processed in cooperation with Simon Buckley. John Howell assisted with detailed knowledge about the regional geology in Utah, helped choose the scanning locations in Utah, and supervised the geological interpretation of the results.

- **Paper 2:** Kurz, Tobias H., Buckley, Simon J., Howell, John A., and Schneider, Danilo: **Integration of panoramic hyperspectral imaging with terrestrial lidar data.** *Submitted to The Photogrammetric Record*

I am responsible for the processing and analysis of the hyperspectral data and for preparing and writing the manuscript. Simon Buckley processed the lidar data. Data

integration and the photogrammetric analysis were carried out in collaboration with Danilo Schneider and Simon Buckley.

• Paper 3: Kurz, Tobias H., Buckley, Simon J., and Howell, John A.: **Remote lithological mapping of geological outcrops using close range hyperspectral imaging**. S*ubmitted to the Journal of the Geological Society, London*

I am responsible for the processing, analysis and interpretation of the hyperspectral data and for preparing and writing the manuscript. The lidar data were processed by Simon Buckley. John Howell provided detailed knowledge about the regional geology in Utah and assisted with the geological interpretation of the spectral and lidar data.

• Paper 4: Kurz, Tobias H., Dewit, Julie, Buckley, Simon J., Thurmond, John B., Hunt, David W., and Swennen, Rudy: **Hyperspectral image analysis of different carbonate lithologies (limestone, karst, hydrothermal dolomites): the Pozalagua Quarry case study (Cantabria, NW Spain).** *Accepted by Sedimentology (Note: main revisions are incorporated, but final text editing was not completed prior to submission of this thesis)*

I am responsible for the processing, analysis and interpretation of the hyperspectral data. Processing of the lidar data and the data fusion were carried out by Simon Buckley. The diagenetic history of the Pozalagua quarry and the analysis of the geochemical data (ICP-OES) were carried out by Rudy Swennen and Julie Dewit. The spectral image products have been geologically interpreted in cooperation with Rudy Swennen and Julie Dewit. While Rudy Swennen authored mainly the section about the geological settings, the description of the digenetic features and the geochemical analysis, I wrote the parts about image spectrometry in carbonates and the spectral data processing, analysis and interpretation. The introduction, the image characteristics of sedimentary and diagenetic features, as well as the discussion and conclusions have been authored collectively. I am responsible for the final manuscript.

Bergen 18th October 2010

Important definitions

Some terminology is used by different research communities with a slightly different meaning because an official definition is lacking. Other terms are well known and used by a specific research community but might be widely unknown in other disciplines. Since this thesis covers cross-discipline issues, relevant "key-terms" are briefly described and defined in the context of this work.

Reflectance nomenclature and terminology

Schaepman-Strub et al. (2006) noted a source of error and uncertainty in analysing reflectance quantities, due to an ambiguous or erroneous usage of reflectance terminology. The physically-based nomenclature and terminology used to describe reflectance problems were proposed by Nicodemus et al. (1977). One of the essential quantities in remote sensing is reflectance, defined as the ratio between incident and backscattered radiance. However, reflectance can also express different quantities depending on the incident and reflected beam configuration. Three general beam geometries are distinguished: directional, conical and hemispherical (Schaepman-Strub et al., 2006). To specify a reflectance quantity, the geometry of the incoming radiance is named at first, followed by the geometry of the reflected radiance for example *hemispherical-directional reflectance*. Identical incident and reflected beam geometry is expressed by the prefix *"bi"*, for example *bidirectional*. The reflectance terminology was adapted to remote sensing applications by Martonchik et al. (2000), who involved diffuse and direct sky illumination. The beam geometry corresponds to the amount of directional and diffuse radiation received and backscattered by a ground pixel. The *bihemispherical reflectance* is also referred to as *albedo*. Some authors also use the term *albedo* to describe directional-hemispherical and conical-hemispherical reflectance. *Bidirectional reflectance* is required to estimate the so called *bidirectional reflectance distribution function* (*BRDF*) which is used as a common concept to describe the reflection behaviour of non-lambertian surfaces (Nicodemus et al., 1977).

Close-range / terrestrial / ground-based

The terms *close-range*, *terrestrial* and *ground-based* are used in this work as synonyms, to express that the scanning is applied with instruments mounted on a tripod, and to distinguish from airborne and spaceborne applications. Whereas the photogrammetric and geomatics communities uses *close-range* or *terrestrial* in contrast to airborne/spaceborne applications, the remote sensing community uses the terms *terrestrial* and *extraterrestrial* to distinguish between observations of the earth from observations of other space objects.

Hyperspectral imaging

Although the terms *imaging spectrometry*, *imaging spectroscopy* and *hyperspectral imaging* have by direct translation a slightly different meaning (spectrometry – "measuring", spectroscopy – "observing", hyperspectral – "many bands"), they are used as synonyms in the remote sensing community and also in this work. The term *imaging spectrometry* was introduce by Goetz et al. (1985) to emphasize that spectral data in the form of complete and continuous spectral curves are used, which are comparable to laboratory spectra and allow the measurement and analysis of single absorption features. Absorption features are also referred to as absorption bands. This enables data analysis by deterministic rather than statistical approaches.

Laser scanning / lidar

Laser scanning is also known as *lidar* (also written as *LIDAR* or *LiDAR*) and is the acronym for **li**ght **d**etection **a**nd **r**anging. *Laser* and *lidar scanning* are used as synonyms in this work. Some authors use also the term *laser radar* or the acronyms *ladar* or *LADAR* (**la**ser **d**etection **a**nd **r**anging) for laser scanning. However, laser scanning and radar (radio detection and ranging) should be distinguished since both approaches uses different frequencies of electromagnetic radiation, which result in different properties of these methods. Laser uses frequencies between c. 10^{12} - 10^{16} Hz which equates to wavelength between c. 0.05-30 µm (ultraviolet to infrared light). Radar instead utilises microwaves and radio waves with frequencies between

c. 10^8 - 10^{11} Hz which equates to wavelength between c. 0.01-10 m. The terms *laser radar* or *ladar* are not used in this work.

Outcrop

In geological field studies, rock exposures that allow geological observation, measurement and analysis are referred to as *outcrops*. Excellent conditions are preferred, meaning that in general the locations are free of soil and vegetation coverage, and that observations are not contaminated by weathered crust. The dimensions of the outcrop have to match the study purpose and can vary from metre-scale to tens or even hundreds of kilometres. Outcrops can be either vertically or horizontally oriented; however, for detailed field studies the bulk of outcrops are vertical cliff sections.

Texturing / texture mapping

In this work *texturing* (also known as *texture mapping*) is used in a photogrammetric or computer graphics context. Texturing is performed when a 2D image, for example a photograph, is integrated with a digital 3D model. The images are draped onto the surfaces resulting in coloured 3D models. In GIS and remote sensing applications, texture often refers to the pattern of an object, for example to distinguish roofing materials by different image patterns. Texture in a geologic-petrographic context refers to the geometric aspects amongst the component particles or crystal grains of a rock.

VIS / NIR / SWIR / VNIR

The classification of the electromagnetic spectrum on the basis of wavelength (or frequency) is not standardised. In this work the reflected part (0.4-3 µm) of the solar radiation which encompasses the relevant spectra in this work is subdivided as follows (see Fig 1 in the Introduction): *visible light* (*VIS*): 0.4-0.74 µm; *near infrared* (*NIR*): 0.74-1.4 µm; *short wave infrared* (*SWIR*): 1.4-3.0 µm. The abbreviation *VNIR* summarised the visible and near infrared spectral range. Other common subdivisions of infrared light refers to near infrared (NIR) 0.7-3.0 µm, mid infrared (MIR) 3.0-

30 μm, and far infrared (FIR) 30-1000 μm. Infrared light with a wavelength greater than 3 μm is mainly emitted instead of reflected and is therefore referred to as thermal infrared (TIR).

Abbreviations

3D / 2D	three dimensional / two dimensional
ASTER	Advanced Spaceborne Thermal Emission and Reflection Radiometer
AVIRIS	Airborne Visible Infrared Imaging Spectrometer
CASI	Compact Airborne Spectrographic Imager
CCD	charge coupled device
CP	control point
EL	Empirical Line correction
ENVI	Environment for Visualizing Images (processing software for spectral images, developed by *ITT Visual Information Solutions*)
FLAASH	Fast Line-of-sight Atmospheric Analysis of Spectral Hypercubes (atmospheric correction module implemented in ENVI)
FOV	field of view
GIS	Geographical Information System
GS	ground sample
HyMAP	Hyperspectral Mapper
iFOV	instantaneous field of view (FOV of one CCD-element)
IR	infrared (light)
JHU	Johns Hopkins University
Landsat TM	Landsat Thematic Mapper
laser	**l**ight **a**mplification by **s**timulated **e**mission of **r**adiation
lidar	**li**ght **d**etection **a**nd **r**anging (synonym to *laser scanning*)
MNF	Maximum Noise Fraction Transform

MTMF	Mixture Tuned Matched Filtering
NIR	near infrared (light)
RGB	red, green, blue
Radar	**Ra**dio **D**etection **a**nd **R**anging also **R**adio **A**ircraft **D**etection **a**nd **R**anging
SAM	Spectral Angle Mapper
SFF	Spectral Feature Fitting
SNR	signal to noise ratio
SPOT	Satellite Pour l'Observation de la Terre
SWIR	short wave infrared (light)
TIR	thermal infrared (light)
TLS	terrestrial laser scanning
USGS	U.S. Geological Survey
VNIR	visible and near infrared (light)
VOM	virtual outcrop model

Introduction

1. Introduction

Within the geosciences, geological outcrops are commonly the focus for collecting geospatial data, including the measurement of geometric parameters and the mapping of mineralogy and lithology. Near-vertical cliff sections, which are often not completely accessible, provide the bulk of geological outcrops used for detailed field studies. Conventional field methods collect data from accessible and representative areas, using methods such as sedimentary logging, hand specimen description, photographraphy and sampling. These methods are frequently hampered by the fact that measurements are only possible at discrete points, and spatial correlation between different cliff sections is difficult. Furthermore, large geometric structures are challenging to access. Geochemical properties of the mineralogy and lithology are limited to macroscopic observations in the field and for more detailed analysis, specimens need to be analysed by laboratory methods, which is time consuming and expensive. Using conventional field methods, the evaluation of large outcrops (which may be kilometres in extent) is costly and the correlation and visualisation of different data types is challenging.

Field-based geoscience studies have been significantly enhanced by new digital spatial data collection technology, which provides a more efficient means of data collection, analysis and visualisation than conventional geological mapping (McCaffrey et al., 2005). Using these techniques, the integration of different data types has been facilitated, in a more quantitative manner, and with high accuracy.

1.1. Current state of research

A number of different approaches have been developed to enable the collection of geospatial data in a non-contact manner, primarily from airborne or spaceborne platforms. Airborne laser scanning has become an alternative to in-situ surveying and aerial photogrammetric techniques are used for obtaining elevation data in an accurate and efficient manner (e.g. Axelsson, 1999). In this method, the time delay between an emitted and backscattered laser beam is utilized for range measurements

(Heritage and Large, 2009), and an angular component allows the determination of 3D point coordinates. By collecting a high number of points, complex surfaces can be modelled. Applied from aircrafts, lidar technology is utilised to represent the topography of the Earth surface as digital elevation models with high resolution (Wehr and Lohr, 1999).

For near-vertical surfaces, terrestrial laser scanning using a close range instrument setting has been developed, and is used in many engineering, industrial and cultural heritage applications (Fröhlich and Mettenleiter, 2004; Slob and Hack, 2004). Applied to geoscience problems, terrestrial laser scanning has become a key development for geological field studies (Bellian et al., 2005; McCaffrey et al., 2005; Buckley et al., 2008). This method allows the shape and form of vertical outcrops to be captured as digital 3D models in an efficient and very accurate manner. To enhance the interpretability, in many geological applications terrestrial laser scanning systems are equipped with a high resolution digital camera to allow colouring and texturing of the lidar derived 3D models with photographs (Bellian et al., 2005; Buckley et al., 2008). The resulting photo-realistic 3D models, also termed virtual outcrop models (VOMs), allow accurate geometric measurements to be made, and provide a platform for visualisation and spatial correlation. Ancillary data, such as sedimentary logs, can also be integrated (Bellian et al., 2005; Enge et al., 2007; Buckley et al., 2010). While lidar data provide accurate geometric information, the extraction of the mineralogy and lithology is limited to the single spectral band provided by the laser and the visible light of the photographs. Adequate methods to complement VOMs with reliable geochemical information in a non-contact manner, allowing the analysis of complex surface compositions, have not yet been developed.

Remote sensing systems measure electromagnetic radiation, utilising the passive solar illumination as an energy source. In geology this has been used for regional mapping of mineralogy and lithology, either from airborne or spaceborne platforms. This method is applied to many different geological problems for instance in geomorphologic and landform studies (Short and Blair, 1986), structural and deformation analysis (Kurz et al., 2007), mineral (Debba et al., 2009) and

hydrocarbon (Berger, 1994) exploration or environmental studies (van der Werff et al., 2008).

For reflectance spectroscopy, the solar reflection range with wavelength between 0.3-2.5 µm is measured, which is largely transmitted through the atmosphere. Earth observers such as Landsat TM, ASTER or SPOT collect a relatively small number of broad (commonly 100-200 nm wide) often discontinuous spectral bands. Since these imagers have a relatively low spectral resolution, resulting in smoothed reflectance characteristics of the surface, they are also termed multispectral sensors (Fig 1). Instead, modern hyperspectral sensors such as AVIRIS, CASI, HyMAP (airborne) or Hyperion (spaceborne) acquire up to hundreds of very narrow spectral bands, usually between 5-15 nm wide, which results in near-continuous spectral curves for each image pixel (Fig 1). Since many earth surface materials have diagnostic absorption features that are 20-40 nm wide (Hunt, 1980; Clark et al., 1990), the high spectral resolution provided by hyperspectral sensors allows detailed analysis of reflectance properties. Using hyperspectral data, imaging spectrometry (Goetz et al., 1985) can be applied, enabling the application of more deterministic approaches, sub-pixel fractions, and a generally more quantitative approach to analysing surface composition.

Imaging spectrometry from airborne/spaceborne platforms is an established method and has been applied to many geological problems. Since the amount of literature is extensive only a few examples, mostly related to sediments, are given. Bowen et al. (2007) analysed fluid-flow pathways in altered Navajo sandstone (Utah) by mapping variations of iron oxides, carbonate and clay content using HyMap data and spectral measurements from the ground. Harris et al. (2005) applied Minimum Noise Fraction (MNF) transformed image products, derived from airborne hyperspectral data, for regional mapping of gneissic-granitoid basement, sandstones and volcanic rocks in northern Canada. Leverington (2010) compared the results of regional geological mapping in an arctic environment (Melville Island, Canada) derived from Landsat and Hyperion data, which differ in spectral and spatial resolutions. In that study, in addition to bedrocks, sandstone, mudstone and limestone units were spectrally

separated. Windeler and Lyon (1991) classified limestone and hydrothermal dolomite from airborne imagery. Due to the presence of a host of minerals with well understood spectral properties including carbonate and clay minerals, the Cuprite area (Nevada, US) has been utilised by various authors (e.g. Kruse et al., 1990; Chen et al., 2010) as a test site for evaluating sensor calibrations and spectral mapping methods.

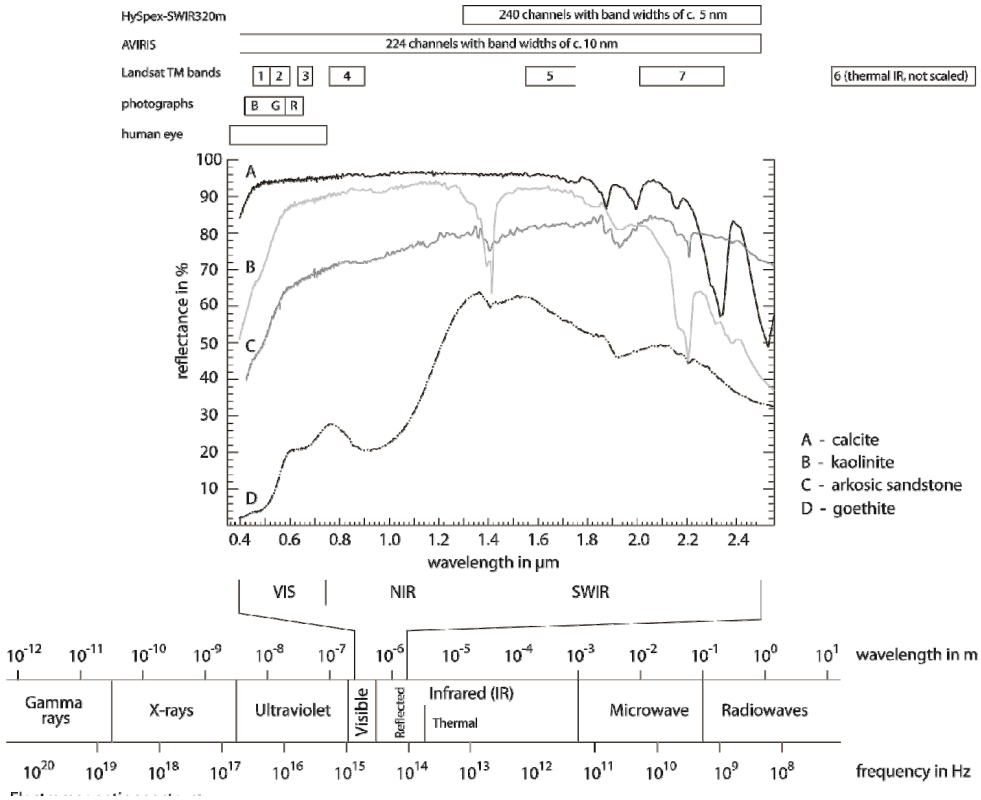

Fig 1 Spectral range and resolution of the Landsat, AVIRIS, HySpex SWIR-320m sensors and conventional photographs. The effect of the spectral resolution for mineral and rock analysis is illustrated by four spectral curves from the USGS spectral library (Clark et al., 1993) and the JHU spectral library (www1; Baldridge et al., 2009).

1.2. Objectives

The aim of this study is to apply imaging spectrometry with a close-range instrument, to enable data acquisition and analysis from near-vertical outcrops, ultimately to complement 3D models derived from terrestrial lidar data with reliable geochemical information. The HySpex SWIR-320m sensor, developed recently by Norsk Elektro Optikk AS is used. This instrument operates solely in the infrared wavelength range of 1.3-2.5 μm. The main objectives of this work are:

1. Evaluate the potential of close-range hyperspectral imaging for geological outcrop studies.

2. Assess instrumentation and scan configuration suitable for geological field applications.

3. Evaluate the photogrammetric performance of the HySpex SWIR-320m camera in close-range geological field applications.

4. Integrate close-range hyperspectral imaging with terrestrial lidar models in a photogrammetric correct manner.

5. Apply close-range hyperspectral imaging to geological case studies with different geological environments.

1.3. Terrestrial laser scanning in geosciences

The benefits provided by an integrated data collection of field data with TLS are used in a number of applications in geosciences. To improve the understanding of erosional processes TLS has been utilized for monitoring coastal cliff evolution (Lim et al., 2005) and landslides (Rowlands et al., 2003). Fault and fracture analysis from terrestrial lidar data are demonstrated by Olariu et al. (2008). Milan (2009) determines grain sizes of gravel-beds from TLS to extract surface roughness and topography data which are required to model and predict flow mechanics of gravel-bed rivers in a more accurate way. Another field in which TLS has been successfully

applied is the analysis of stratigraphic evolution and geometric architecture of sediment systems (Phelps et al., 2008; Enge et al., 2010).

Although the generation of VOMs from TLS is briefly described in Paper 1, two major processing steps are shown in figure 2. After multiple lidar scans have been registered to a common coordinate system, the lidar point cloud is meshed by triangulation to reconstruct the 3D surface. The imagery can be registered to the lidar coordinate system in an automatic manner since the camera is rigidly mounted to the laser scanner. Thus the orientation of the imagery is known. Applying the collinearity condition for frame images (Luhmann et al., 2006), the triangulated lidar surfaces can be textured and coloured with the photographs.

In petroleum geology, VOMs are frequently used in reservoir analogue studies, for building models that give a geometric component in analysing fluid flow and seismic wave propagation through subsurface reservoirs and aquifers (Pringle et al., 2006). Since subsurface data is limited to seismic and drill core data which cannot represent the full geological heterogeneity of subsurface reservoirs, the prediction of fluid flow behaviour is hampered. Surface outcrops are therefore used as reservoir analogues which provide the analysis and quantifications of geometric and mineralogical properties influencing heterogeneities and fluid flow in more detail (Alexander, 1992). Enge et al. (2007) present a workflow for generating geocellular models form VOMs, which are than used to simulate fluid flow through the model to understand how it would behave as a reservoir.

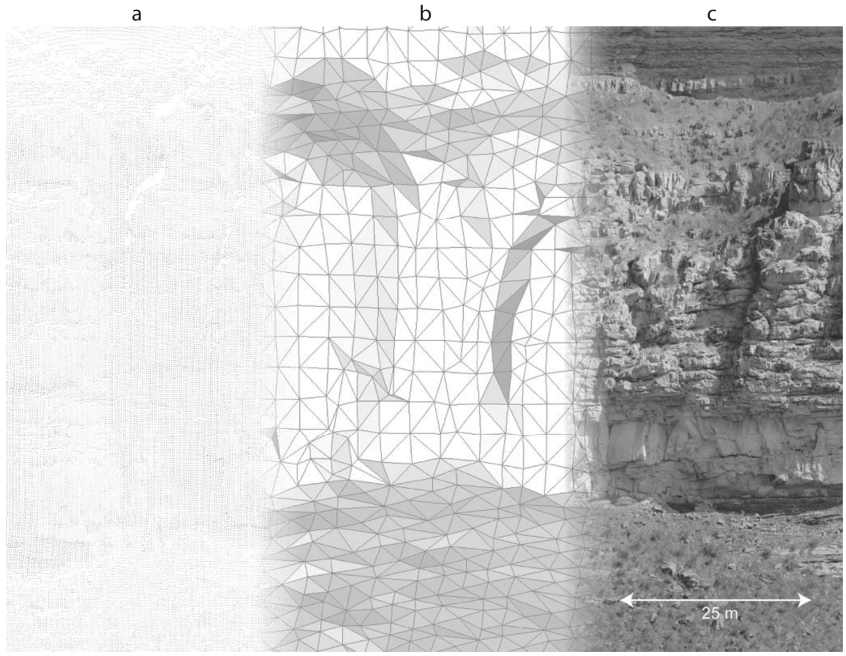

Fig 2 Main processing stages to create a photorealistic lidar model; a: lidar point cloud; b: triangulated (meshed) and decimated point cloud; c: triangulated surface textured with photographs (from Buckley et al., 2008).

1.4. Imaging spectrometry

To extract useful geological information from reflected radiation, the nature and the way electromagnetic radiation interacts with matter needs to be understood. Hunt (1980) gives an excellent introduction to the physical concepts and principles for remote sensing purposes, with a focus on the origin of spectral signatures of minerals. Details of radiative transfer theories, which provide physical and analytical descriptions of scattering, transmittance, absorption and emission processes can be found in Hapke (1981; 1993) and Thomas and Stamnes (2002). In the following section, a brief introduction to the physical principles and concepts of imaging spectrometry in remote sensing applications is given, which may be helpful for a better understanding of the strengths and limitations of this method.

While the wave nature of electromagnetic energy can be described by Maxwell's electromagnetic wave theory, the particulate nature of electromagnetic energy is explained by modern quantum theory based on the Schrodinger wave equations. The

quantum theory is based on the principle that energy is transmitted as indivisible packets referred to as quanta or photons. Spectral sensors collecting the number of photons per wavelength emitted by the material contained within a ground pixel. The number of photons can be transformed into radiance, which expresses the emitted energy per unit of time in a specific direction by a unit of area, measured in watt per steradian per square metre (W sr^{-1} m^{-2}). In spectrometry, the reflectance is commonly the desired quantity determined by calculating the ratio of the irradiance (incident radiance) and backscattered radiance.

1.4.1. Origin of absorption features

The origin of absorption bands in minerals observable in reflectance spectra can be explained by quantum mechanical concepts. The following discussion is based on Hunt (1980). Isolated atoms or ions have discrete energy states. A change of the energy state is referred to as transition. If a photon of a specific wavelength is absorbed or emitted, the energy state is changed. Absorption results in a higher energy state and emission in a lower energy state. Since an absorbed photon of a specific wavelength is usually not emitted at the same wavelength, absorption bands can be generated. Absorption bands within the visible and reflected infrared light are related to electronic and vibrational processes within the crystal lattice. Electronic transition processes require more energy; hence they occur mainly at shorter wavelengths within the VIS and NIR spectrum, and give rise to broad absorption features. Electronic processes in solids are discussed in more detail by Burns (1993a, b). Vibrational processes take place within the infrared spectra (NIR, SWIR and thermal) and result typically in small and sharp absorption bands. Details on vibrational processes in minerals can be found in Farmer (1974) and Gaffey et al. (1993). The position and shape (depth, width and asymmetry) of an absorption feature are controlled primarily by the kind of absorbing ion or molecule and its position within the crystal lattice (e.g. octahedral, tetrahedral site). But also the kind of chemical bond and the elements involved in the bond influence the position and shape of the absorption feature.

Electronic processes

In minerals, electronic transition processes yielding absorption features are related to crystal field effects, conduction bands, charge transfer transition and colour centres. Which processes take effect depends on the chemical bond and the involved elements. Crystal field effects are typically associated with transition metal ions such as Cu, Ni, Co, Mn, Cr, Ti, and particularly Fe, which split and displace the energy of the unfilled *d* orbitals of the isolated atoms into new energy levels, by interaction with the surrounding crystal field. Transitions between these new energy levels are primarily determined by the valence (oxidation) state of the ion (for example Fe^{2+} or Fe^{3+}), its coordination number and site symmetry (octahedral, tetrahedral) and secondarily by the type of the connected ligand (for example metal-oxygen), the extent of distortion of the metal ion site and the metal-legand interatomic distance. Rhodochrosite ($MnCO_3$) is an example where absorption features in the VIS spectra appear due to manganese and crystal field effects (Hunt and Salisbury, 1971). Since iron is a common substitute element and its bonding in a crystal lattice is very active within the VIS, NIR and SWIR spectra, even with low iron concentrations, iron absorption occurs (and is often dominating) in many earth materials.

Some minerals behave as semiconductors, and display properties which are intermediate between those of metals and dielectrics. In such materials conduction bands can be responsible for sharp absorption features. Conduction bands refer to higher energy levels allowing electrons a free movement throughout the crystal lattice whereas valence bands represent lower energy levels where electrons are attached to individual atoms. Conduction and valence bands are divided by the forbidden band (also called forbidden gap), a zone of energies which the electrons may not adopt. Absorption occurs when photons have sufficient energy to excite electrons across the forbidden band. Many sulphides show absorption features related to conduction bands.

Charge transfer transition refers to the specific case where electrons migrate between neighbouring ions without entering the conduction band, and occurs often when metal ions with different oxidation states are present in a mineral. In general, absorption

caused by charge transfer is much stronger (hundreds to thousands of times) than absorption by crystal field effects (Burns, 1993b). The absorption maxima usually occur in the ultraviolet spectra, although the absorption edges may extend into the VIS spectra. Reddish colours of iron oxides and hydroxides are related to charge transfer absorption.

Colour centres are related to the irradiation of an imperfect crystal. Imperfect crystals, caused for example by impurities, can create discrete energy levels. Photon energy can move electrons into the defects, resulting in a change of energy levels. Fluorites show typical absorption related to colour centres.

Vibrational processes

Oscillating small displacements of atoms in a crystal lattice or molecule can be understood in analogy to the oscillation of a spring with attached weights (Clark, 1999). The oscillation frequency of a spring depends on the strength of the spring and the mass of the weights. Analogously, the vibration frequency in a crystal lattice is determined by the bond in the molecule and the mass of each element in the molecule. For molecules with N atoms, 3N-6 independent types of vibration are possible and referred to as fundamental vibration modes (usually labelled with v and a subscribed number, for example v_1, v_2, v_3) which show different oscillation vectors (Clark, 1999).

Stimulated by the fundamental vibration modes, so called overtones and combination tones can occur. Overtones are vibrations with frequencies which have integer multiplications of the fundamental frequencies (labelled and expressed for example by $2v_1$, $3v_1$, $2v_2$). Combination tones are vibrations with frequencies resulting from addition (or subtraction) of the fundamental frequencies (labelled and expressed for example by v_1+v_2, v_2+v_3, $v_1+v_2+v_3$). The fundamental vibration modes and the associated overtones and combination tones can be considered as energy levels of the crystal lattice. By interaction of photons with the vibrational system, energy levels can be changed and absorption can occur.

Absorption related to fundamental vibration occurs usually at longer wavelengths beyond the SWIR spectra. However, diagnostic absorption features within the SWIR range can be generated due to overtones and combination tones for materials with very high fundamental frequencies. Such absorption can be observed for instance if carbonate ions, hydroxyl ions or water are present in a mineral.

The fundamental vibration modes (relevant for remote sensing purposes) of a free carbonate ion (CO_3^{2+}) are shown in figure 3 and table 1. 3D animations of the fundamental vibration motions can be examined at www[1]. A carbonate ion consists of 4 atoms; consequently for N=4, 6 fundamental modes are possible. Fundamental vibration at c. 7 µm and c. 14 µm appear as couples. That means that in each case actually two vibrations with very similar frequencies and respectively with the same vibration modes occur. Vibration with the same mode but a slightly different frequency is termed doubly degenerate and results in a single absorption band, hence only 4 (instead of 6) fundamental vibration modes are listed for carbonate ions in the context of absorption. In carbonates five pronounced absorption bands appear within the SWIR due to overtones and combination tones (Tab 2). The exact position of these band centres depends on the metal ions connected to the carbonate ligand; hence, for example calcite ($CaCO_3$) and dolomite ($CaMg[CO_3]_2$) can be distinguished due to a slight shifting of carbonate absorption features.

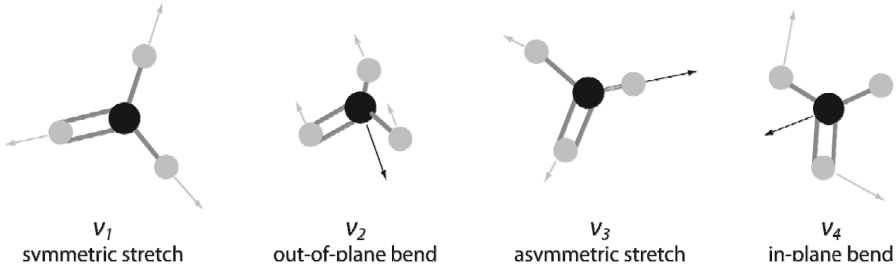

Fig 3 Fundamental vibration modes with motion vectors of a free carbonate ion (CO_3^{2+}) (after www1).

Tab 1 Fundamental vibration modes of a free carbonate ion (Hunt and Salisbury, 1971), considered in remote sensing applications.

Fundamental	Vibrational mode	Wavelength (µm)	Wave number (cm^{-1})	comment
v_1	symmetric stretch	9.25	1080	not IR active
v_2	out-of-plane bend	11.36	880	
v_3	asymmetric stretch	6.99	1430	doubly degenerate
v_4	in-plane bend	13.98	715	doubly degenerate

Tab 2 Absorption features (sorted by strength) of carbonates within the SWIR spectra (Hunt and Salisbury, 1971).

Absorption band	Wavelength (µm)	Wave number (cm^{-1})	Overtones / combination tones
1	2.5 – 2.55	4000-3900	$v_1 + 2v_3$
2	2.30 – 2.35	4350-4250	$3v_3$
3	2.12 – 2.16	4720-4330	$v_1 + 2v_3 + v_4$ or $3v_1 + 2v_4$
4	1.97 – 2.00	5080-5000	$2v_1 + 2v_3$
5	1.85 – 1.87	5400-5350	$v_1 + 3v_3$

1.4.2. Spectral signatures of minerals and rocks

The spectral signatures of minerals and rocks have been studied in detail by numerous authors. Hunt, Salisbury and Lanhoff present a large catalogue of mineral and rock spectra in a series of publications (Hunt et al., 1970-76). Libraries of digital spectra are provided for example by Clark et al. (1993). Hunt (1977) shows the most common absorption features for minerals within the VIS, NIR and SWIR ranges in a single diagram, sorted according to their electronic and vibrational origin (Fig 4). The minerals listed in figure 4 are representative examples. Absorption at similar positions occurs for minerals containing the absorbing ions or molecules at the same position within the crystal lattice.

Rocks are composites of minerals; hence, rock spectra are compositions of individual spectra of its constituent minerals. In general, imaging spectrometry allows semi-quantitative analysis of mineral abundances from rock spectra for example by analysing the intensity of absorption bands (Clark, 1999). However, some minerals such as quartz and feldspar do not possess absorption features within the measured spectral range (VIS, NIR, SWIR). Such minerals are referred to as featureless or

minerals with flat absorption, and cannot be analysed by spectrometry (within the featureless spectral range). Furthermore, specific minerals or an absorbing type such as iron ions, organic material or hydroxyl ions might dominate the rock spectra and hamper the identification of other constituent minerals that have less pronounced absorption properties. Consequently, an analysis in a petrographic manner cannot be obtained from rock spectra. However, in many cases a mineral (or a specific kind of ion or molecule such as hydroxyl ions) with a unique absorption signature can be correlated to a specific lithological unit which can be used to trace and map the lithology. Additionally, abundance and in turn spatial variation can be determined from the rock spectra. Common reflection features in sedimentary rocks are for example often related to carbonate material and hydroxyl, water or iron connected to clay minerals or weathering products (Hunt and Salisbury, 1976).

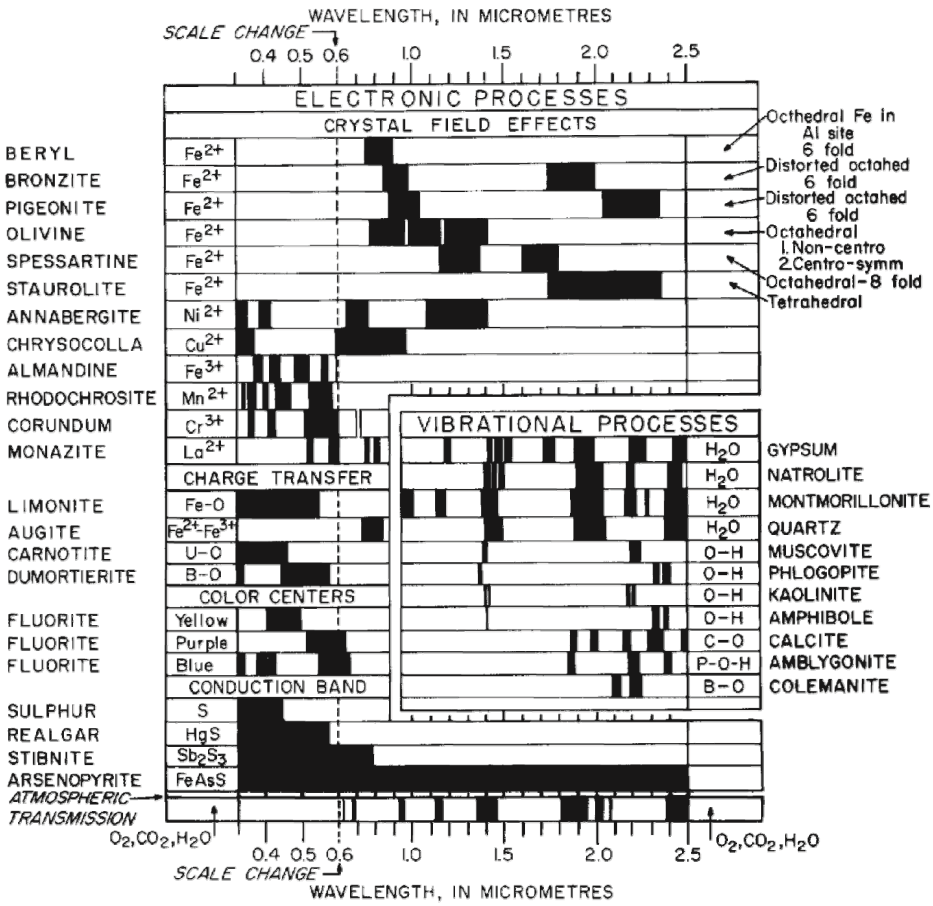

Fig 4 Spectral signature diagram from Hunt (1977).

1.4.3 Factors influencing the spectral response

A number of physical properties can influence and modify the spectral curve of minerals and rocks (Gaffey et al., 1993; Clark, 1999). However, while most of these factors affect the overall brightness or contrast (intensity differences) of the spectral curve, the position of the absorption features are not shifted. Some properties are recognisable in laboratory measurements, such as porosity (Hapke, 2008), but they might not be significant in remote sensing applications, due to low spatial resolution and higher noise levels. Factors such as particle size, mineral mixture, view geometry and surface roughness might influence spectral curves obtained from image scenes (Hapke, 1984; Gaffey et al., 1993). In general, the depth of an absorption feature

indicates the amount of light absorbed and is therefore related to the abundance of the absorber (Clark and Roush, 1984; Clark, 1999). However, the particle size can affect the absorption band intensity (Gaffey et al., 1993). In non-opaque material, the absorption intensity (depth of the absorption band) increases with increased grain or particle size, whereas the overall reflectance decreases (Clark and Roush, 1984; Clark et al., 2003). Larger particles provide a greater internal path - the distance radiation can travel through the material, where photons may be absorbed according to Beers Law.

In general, four different types of spectral mixture need to be distinguished: linear, intimate, molecular mixture and mixing due to coating (Clark, 1999). If materials are optically separate and there is no multiple scattering between the components, the resulting spectrum will be a linear mixture (also termed as spatial mixture), whereas the mixed spectrum is a linear weighted sum of the individual components. Intimate mixture result in complex non-linear mixed spectra due to multiple scattering between materials which are in intimated contacts, such as grains of different minerals in rocks. Molecular mixture occurs on a molecular level when for instance liquids or liquids-solids are mixed together, and can result in band shifts. An example is interlayer water in montmorillonite. In spectra mixed due to coating, each coat acts as a scattering-transmittance layer, with different optical thickness and material-dependent absorption properties.

If spatial separation of different materials can be assumed, and if the spectrum of each component is known (end-member spectra), the fraction of each component present in a pixel can be determined by linear spectral unmixing algorithms. An overview about the concepts and the application of spectral unmixing can be found in Adams et al. (1993), Ichoku & Karnieli (1996) and Keshava & Mustard (2002).

1.4.4. Analysis of absorption features

The wavelength position, the depth and shape of an absorption feature, cannot be directly analysed from the reflectance curve (Clark and Roush, 1984). Before the analysis can be performed, the absorption features need to be isolated from other

effects (Clark et al., 2003; van der Meer, 2004). For example strong atmospheric absorption features often affect adjacent parts of the reflection curve which becomes visible as slopes within the spectra. Hence, absorption features situated within such a slope are distorted (see absorption feature at 1.8 µm in Fig 5).

Absorption in a spectrum consists of two components, the continuum and individual features. The continuum is the background or overall reflectance and can be determined by fitting a convex hull at the top of the spectrum, connecting local maxima (Fig 5). To remove the continuum, the original spectrum is divided by the continuum curve. Consequently, the resulted continuum removed spectrum is normalized to one. Detailed analysis of absorption features, such as the determination of the position, the absorption depth and the shape, are performed using continuum removed spectra. Spectral feature fitting approaches used for spectral mapping or to compare measured spectra with library spectra (Clark et al., 1991; Clark et al., 2003) are based on continuum removed pixel spectra.

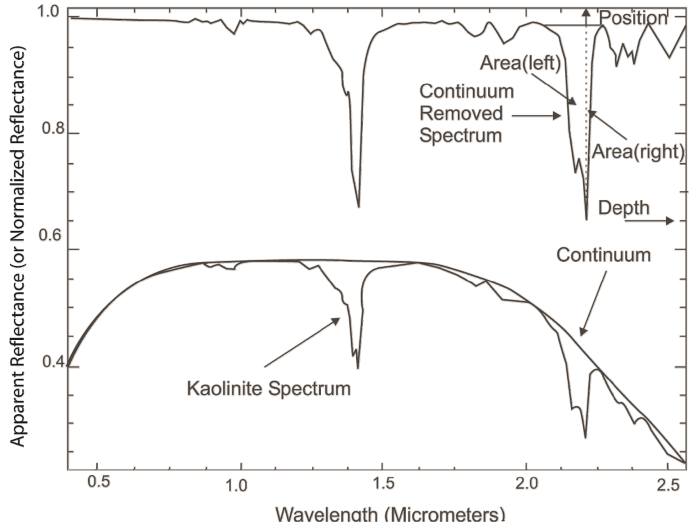

Fig 5 Extraction and analysis of absorption features based on continuum removed spectra (from van der Meer, 2004).

1.4.5. Interaction with atmosphere and adjacencies

In remote sensing applications, the intrinsic radiance of a ground sample (GS) measured by the sensor is influenced by a number of effects. The measured at-sensor radiance is a "mixed-signal" consisting of the directional intrinsic radiance of a GS and additional radiance received by scattering with atmospheric gases and the surrounding area (see Fig 1 in Paper 1). Atmospheric and topographic effects have to be removed to allow quantitative evaluation of remote sensing data (Gao et al., 2009). Imaging spectrometry in remote sensing applications utilises solar energy as the illumination source, while the solar irradiance is significantly reduced by the atmosphere. The available solar energy at the Earth's surface (sea level) is shown in figure 6. Since the composition of the atmosphere is temporally and geographically variable, the local solar irradiance varies. Besides atmospheric gases, aerosols particularly in the lower atmosphere cause significant scattering, and interfere with reflectance measurements. Within the SWIR spectra, strong atmospheric absorption due to water vapour appears between approximately 1.35-1.45 µm, 1.8-1.95 µm and 2.47-3.5 µm. Additionally, two relatively sharp absorption bands appear around 2.01 µm and 2.08 µm due to carbon dioxide (Fig 6). Within these spectral ranges, this atmospheric effect can result in near-total absorption, making affected spectral channels unusable for detecting and evaluating mineral absorption features. Atmospheric correction can be performed in an empirical manner, by using correction parameters based on reference spectra known in the image (Gao et al., 2009). While the processing cost is low, not all atmospheric and topographic effects can be adequately removed. Furthermore, the comparability of the reflectance spectra retrieved from different images is restricted. Alternatively, atmospheric correction can be applied using radiative transfer models to quantify atmospheric and topographic scattering effects in an analytical manner (Richter, 1998; Gao et al., 2009). However, additional data such as the local composition of the atmosphere, optical thickness and illumination-viewing geometry are required, and the processing can be costly and time consuming.

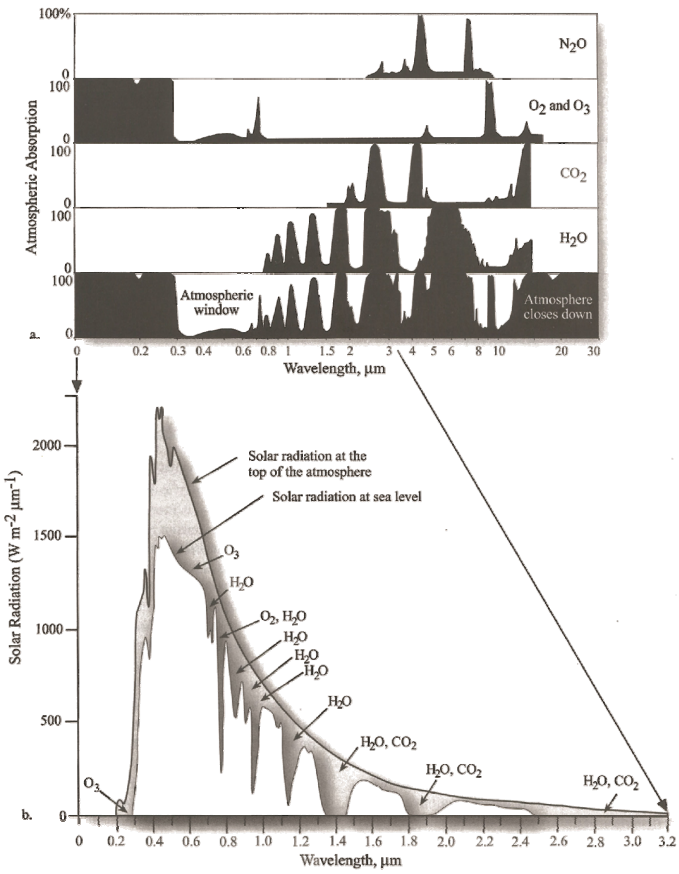

Fig 6 Solar radiation at the top of the atmosphere and at sea level, with absorption by various atmospheric gases (from Jensen, 2007).

1.5. Instrumentation

1.5.1. Hyperspectral imager HySpex SWIR-320m

The HySpex SWIR-320m scanning system developed by *Norsk Elektro Optikk AS* consists of the sensor head, a rotation stage, various acquisition devices (frame grabber, rotation stage controller, camera link and current transformers), and a field laptop (Fig 7). This imager was primarily developed for industrial applications, for which the size, weight and the energy consumption is not a critical issue. A lightweight generator is used to provide power supply in the field.

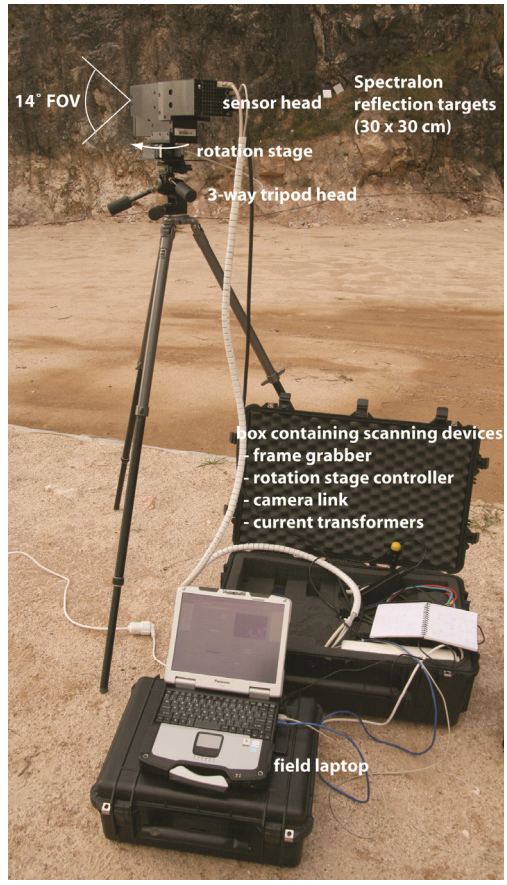

Fig 7 HySpex SWIR-320m scanning system.

The HySpex SWIR-320m imager operates within the infrared part of the electromagnetic spectrum, between 1.3-2.5 µm. 240 bands are collected, with an average band width of 5 nm (full width at half maximum). Specifications of the HySpex SWIR-320m sensor are shown in table 3. Since many rock forming minerals provide diagnostic absorption bands within infrared light and with absorption band widths in the order of 20 nm (Hunt, 1980; Clark et al., 1990), this instrument is suitable for many geological applications and for detailed analysis of absorption properties. To enable close-range image acquisition, the instrument is integrated with a rotation stage and mounted on a tripod. Images are acquired by rotating a vertical sensor line with 320 spatial pixels (pushbroom scanning) which provides a field of view (FOV) across track of 14°. Although panoramic images with a FOV along track

of 360 º can be acquired, image acquisition is usually carried out with a smaller panoramic angle to ensure uniform illumination condition in a scene.

The optical elements of the sensor are shown in figure 8. With the regular scanning mode, the inbuilt lens provides scanning ranges from c. 15 m to infinity. The inbuilt lens has a focal length of c. 40 mm which results in an image pixel resolution of 3.25 cm at 50 m scanning range. Additional close-range lenses can optionally be mounted to enable scanning at shorter ranges than 15 m. However, these lenses have a very low depth of field, which can limit their practical usage in the field. More details about the scanner specifications are described in Papers 1 and 2.

Table 3. Specifications of the HySpex SWIR-320m imager.

Detector	HgCdTe (320 x 256 pixels)
Spectral range	1.3-2.5 µm
Spectral sampling	~5 nm
Number of bands	240
Digitisation	14 bit
Spatial pixels in the vertical line	320
Field of view across track (sensor line)	14°
Pixel field of view along/across track	0.75 mrad, 0.75 mrad
Focal length	~40 mm
Focal plane array cooling temperature	~195 K
Image storage format	band interleaved by line (BIL)

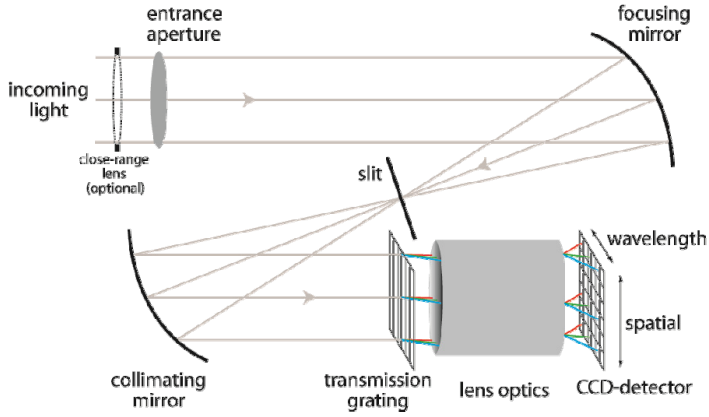

Fig 8 Optical unit of the HySpex sensor (after HySpex user manual); close-range lenses can optionally be mounted to enable scanning at distances less than 15m.

1.5.2. Terrestrial lidar system Riegl LMS-Z420i

The lidar data were collected using the Riegl LMS-Z420i scanning system from *Riegl Laser Measurement Systems GmbH* (Fig 9). The scanner operates on the principle of time-of-flight and provides range measurements from 2 m up to 800 m (at 80 % reflectivity). 3D images with a FOV of 360º x 80º and a quoted single measurement precision of 0.01 m can be acquired. The data acquisition rate is up to 12,000 points per second. The point grid resolution can be user defined at which the maximal angle resolution is 0.002º in the vertical and 0.0025º in the horizontal direction. A high resolution digital camera can be mounted rigidly on top of the scanner (Fig 9) to allow automatic registration of the imagery and to enable colouring and texturing of the lidar point cloud with the photographs. A single-frequency GPS instrument which collects data relative to a base station can additionally be mounted on the scanner. However, since the registration of the lidar models in a global geographic coordinate system was not essential in this work, processing of the GPS data is omitted. This instrument has been designed for rapid data acquisition under demanding field conditions and its performance is well-suited for many earth science applications.

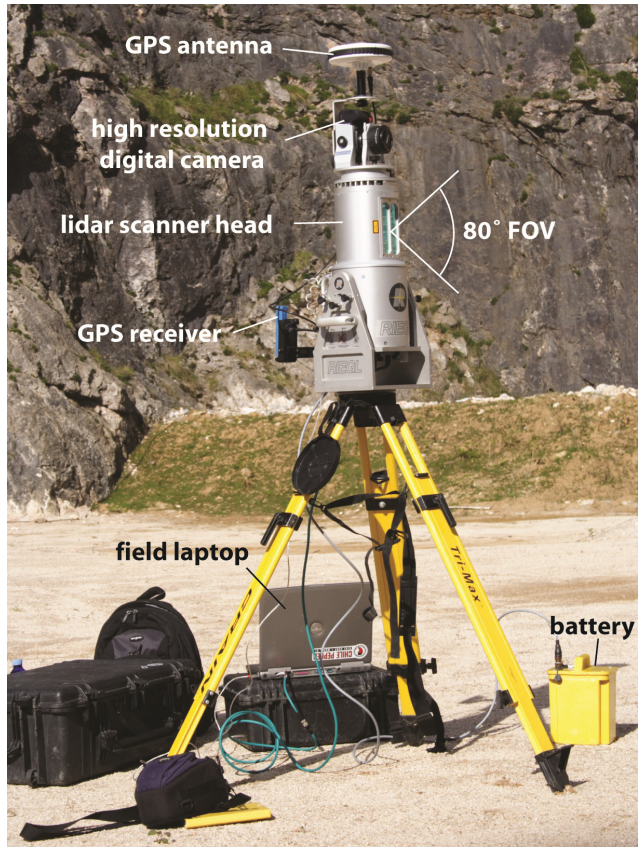

Fig 9 Riegl LMS-Z420i terrestrial laser scanning system.

1.5.3. Scanning setup

To facilitate the data integration, the hyperspectral and lidar data were collected simultaneously with similar scanning views and scanning angles. Details on the data collection are described in Paper 1 and 2. Figure 10 shows a typical instrument setup in the field. Retro-reflective targets (cylinder and tape), shown in figure 11 (a and b), were used for control point (CP) measurement to support photogrammetric processing. Retro-reflective tape was also used to mark sample locations which could then be located in the lidar models as well as in the spectral images. Calibrated Spectralon diffuse reflector targets (Fig 11c) were placed in accessible cliff sections and scanned with the spectral imager to obtain reference spectra for spectral image corrections.

Figure 12 shows a scanning setup with the 1 m lens to acquire spectra for rock samples in the field. The rock samples spectra were intended to ensure pure end-member spectra and to support the spectral mapping of the scanned cliff sections. However, images collected with the 1 m lens in the field were characterized by extremely low signal to noise ratios. Sample spectra retrieved from these images could not be utilised for spectral mapping of the outcrops. The origin of the high noise level could not be completely explained, and must be analysed further.

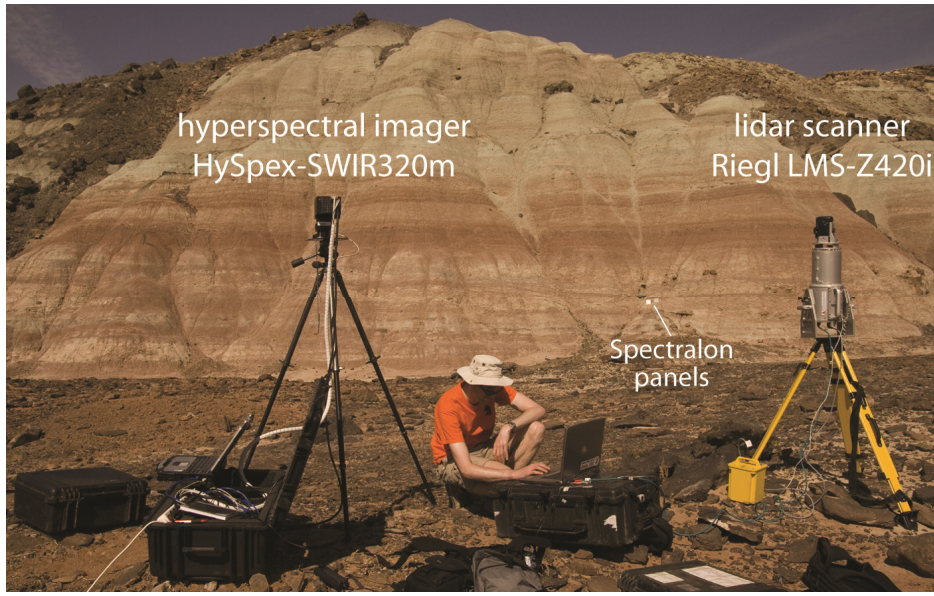

Fig 10 Instrument setup in the field.

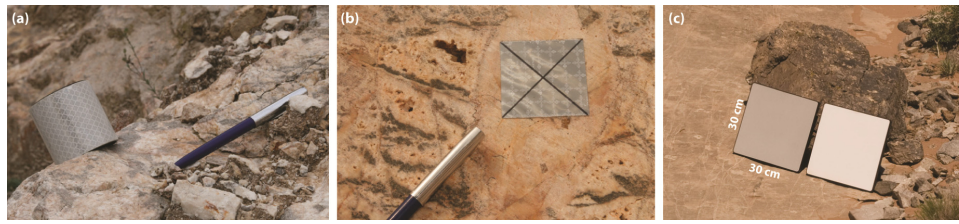

Fig 11 Reflection targets. (a) Cylindrical retro-reflective targets for semi-automatic control point collection (b) Sample locations marked with retro-reflective tape (c) Spectralon reflection panels for spectral image calibration.

Fig 12 Scanning setup with the 1 m lens to collect rock sample spectra in the field.

References

Adams, J.B., Smith, M.O., and Gillespie, A.R., 1993. Imaging Spectrometry: Interpretation based on spectral mixture analysis. In: Pieters, C.M., and Englert, P.A.J., (eds.), Remote Geochemical Analysis: Elemental and Mineralogical Composition, Topics in remote sensing 4. Cambridge, Cambridge University Press, pp. 121-166.

Alexander, J., 1992. A discussion on the use of analogues for reservoir geology. In Ashton, M. (ed.) Advances in Reservoir Geology. Geological Society of London, Special Publications, v. 69, pp. 175-194.

Axelsson, P., 1999. Processing of laser scanner data - algorithms and applications. ISPRS Journal of Photogrammetry and Remote Sensing, v. 54 (2-3), pp. 138-147.

Baldridge, A.M., Hook, S.J., Grove, C.I., and G., R., 2009. The ASTER spectral library version 2.0. Remote Sensing of Environment v. 113 (4), pp. 711-715.

Bellian, J.A., Kerans, C., and Jennette, D.C., 2005. Digital outcrop models: Applications of terrestrial scanning lidar technology in stratigraphic modeling. Journal of Sedimentary Research, v. 75 (2), pp. 166-176.

Berger, Z., 1994. Satellite hydrocarbon exploration: interpretation and integration techniques Berlin, Springer, 319 pp.

Bowen, B.B., Martini, B.A., Chan, M.A., and Parry, W.T., 2007. Reflectance spectroscopic mapping of diagenetic heterogeneities and fluid-flow pathways in the Jurassic Navajo Sandstone. AAPG Bulletin, v. 91 (2), pp. 173-190.

Buckley, S.J., Enge, H.D., Carlsson, C., and Howell, J.A., 2010. Terrestrial laser scanning for use in virtual outcrop geology. The Photogrammetric Record, v. 25 (131), pp. 225-239.

Buckley, S.J., Howell, J.A., Enge, H.D., and Kurz, T.H., 2008. Terrestrial laser scanning in geology: data acquisition, processing and accuracy considerations. Journal of the Geological Society, London, v. 165 (3), pp. 625-638.

Burns, R.G., 1993a. Mineralogical applications of crystal field theory. (2nd edn.), Cambridge, Cambridge University Press, 551 pp.

Burns, R.G., 1993b. Origin of electronic spectra of minerals in the visible to near-infrared region. In: Pieters, C.M., and Englert, P.A.J., (eds.), Remote geochemical analysis: elemental and mineralogical composition. Topics in remote sensing 4. Cambridge, Cambridge University Press, pp. 3-29.

Chen, X., Warner, T.A., and Campagna, D.J., 2010. Integrating visible, near-infrared and short-wave infrared hyperspectral and multispectral thermal imagery for geological mapping at Cuprite, Nevada: a rule-based system. International Journal of Remote Sensing, v. 31 (7), pp. 1733–1752.

Clark, R.N., 1999. Chapter 1: Spectroscopy of Rocks and Minerals, and Principles of Spectroscopy. In: Rencz, A.N., and Ryerson, R.A., (eds.), Manual of Remote

Sensing, Volume 3, Remote Sensing for the Earth Sciences (3rd end.). New York, John Wiley and Sons, pp. 3-58.

Clark, R.N., King, T.V.V., Klejwa, M., Swayze, G.A., and Vergo, N., 1990. High spectral resolution reflectance spectroscopy of minerals. Journal of Geophysical Research, B: Solid Earth, v. 95 (8), pp. 12653-12680.

Clark, R.N., and Roush, T.L., 1984. Reflectance spectroscopy: quantitative analysis techniques for remote sensing applications. Journal of Geophysical Research, v. 89 (B7), pp. 6329-6340.

Clark, R.N., Swayze, G.A., Gallagher, A., Gorelick, N., and Kruse, F.A., 1991. Mapping with imaging spectrometer data using the complete band shape least-squares algorithm simultaneously fit to multiple spectral features from multiple materials. In: Proceedings, 3rd Airborne Visible/Infrared Imaging Spectrometer (AVIRIS) workshop, JPL publication 91-28, pp. 2-3.

Clark, R.N., Swayze, G.A., Gallagher, A.J., King, T.V.V., and Calvin, W.M., 1993. The U. S. Geological Survey, Digital Spectral Library: Version 1: 0.2 to 3.0 microns, U.S. Geological Survey Open File Report 93-592, 1340 pages.

Clark, R.N., Swayze, G.A., Livo, K.E., Kokaly, R.F., Sutley, S.J., Dalton, J.B., McDougal, R.R., and Gent, C.A., 2003. Imaging spectroscopy: Earth and planetary remote sensing with the USGS Tetracorder and expert systems. Journal of Geophysical Research, G: Planets, v. 108 (12), pp. 5-1 - 5-44.

Debba, P., Carranza, E.J.M., Stein, A., and van der Meer, F.D., 2009. Deriving optimal exploration target zones on mineral prospectivity maps. Mathematical Geosciences, v. 41 (4), pp. 421-446, doi: 10.1007/s11004-008-9181-5.

Enge, H.D., Buckley, S.J., Rotevatn, A., and Howell, J.A., 2007. From outcrop to reservoir simulation model: workflow and procedures. Geosphere, v. 3 (6), pp. 469-490, doi: 10.1130/ges00099.1.

Enge, H.D., Howell, J.A., and Buckley, S.J., 2010. Quantifying clinothem geometry in a forced-regressive river-dominated delta, Panther Tongue Member, Utah, USA. Sedimentology, v. 57 (7), pp. 1750-1770, doi: 10.1111/j.1365-3091.2010.01164.x.

Farmer, V.C., (ed.) 1974. The Infrared spectra of minerals. London, Mineralogical Society, 539 pp.

Fröhlich, C., and Mettenleiter, M., 2004. Terrestrial laser scanning - new perspectives in 3D surveying. In: Laser-scanners for forest and landscape assessment. Proceedings of the ISPRS working group VIII/2, Freiburg, Germany, International Archives of Photogrammetry, Remote Sensing and Spatial Information Sciences XXXVI-8/W2, pp. 7-13.

Gaffey, S.J., McFadden, L.A., Nash, D., and Pieters, C.M., 1993. Ultraviolet, visible, and near-infrared reflectance spectroscopy: laboratory spectra of geologic materials. In: Pieters, C.M., and Englert, P.A.J., (eds.), Remote Geochemical Analysis: Elemental and Mineralogical Composition, Topics in remote sensing 4, Cambridge, Cambridge University Press, pp. 43-77.

Gao, B.-C., Marcos, J.M., Curtiss, O.D., and Alexander, F.H.G., 2009. Atmospheric correction algorithms for hyperspectral remote sensing data of land and ocean. Remote Sensing of Environment, v. 113 (Supplement 1), pp. S17–S24.

Goetz, A.F.H., Vane, G., Solomon, J.E., and Rock, B.N., 1985. Imaging spectrometry for earth remote sensing. Science, v. 228 (4704), pp. 1147-1153.

Hapke, B., 1981. Bidirectional reflectance spectroscopy 1. Theory. Journal of Geophysical Research v. 86 (B4), pp. 3039-3054.

Hapke, B., 1984. Bidirectional reflectance spectroscopy 3. Correction for macroscopic roughness. Icarus, v. 59 (1), pp. 41-59.

Hapke, B., 1993. Theory of reflectance and emittance spectroscopy. Cambridge, Cambridge University Press, 455 pp.

Hapke, B., 2008. Bidirectional reflectance spectroscopy 6. Effects of porosity. Icarus, v. 195 (2), pp. 918-926.

Harris, J., Rogge, D., Hitchcock, R., Ijewliw, O., and Wright, D., 2005. Mapping lithology in Canada's Arctic: application of hyperspectral data using the minimum noise fraction transformation and matched filtering. Canadian Journal of Earth Sciences, v. 42 (12), pp. 2173-2193.

Heritage, G., and Large, A., 2009. Principle of 3D laser scanning. In: Heritage, G., and Large, A., (eds.), Laser scanning for the environmental sciences. Chichester, Wiley-Blackwell, pp. 21-34.

Hunt, G.R., 1977. Spectral signatures of particulate minerals in the visible and near infrared. Geophysics, v. 42 (3), pp. 501-513.

Hunt, G.R., 1980. Electromagnetic radiation: the communication link in remote sensing. In: Siegal, B.S., and Gillespie, A.R., (eds.), Remote sensing in geology. New York, John Wiley & Sons, pp. 5-45.

Hunt, G.R., and Salisbury, J.W., 1971. Visible and near-infrared spectra of minerals and rocks: II. Carbonates. Modern Geology, v. 2 (1), pp. 23-30.

Hunt, G.R., and Salisbury, J.W., 1976. Visible and near-infrared spectra of minerals and rocks: XI. Sedimentary rocks. Modern Geology, v. 5 (4), pp. 211-217.

Hunt, G.R., Salisbury, J.W., and Lenhoff, C.J., 1970-76. Visible and near-infrared spectra of minerals and rocks I - XII (serial papers). Modern Geology, v. 1-5.

Ichoku, C., and Karnieli, A., 1996. A review of mixture modeling techniques for sub-pixel land cover estimation. Remote Sensing Reviews, v. 13 (3-4), pp. 161-186.

Jensen, J.R., 2007. Remote Sensing of the Environment and Earth Resource Perspective. (2nd edn.), Upper Saddle River, NJ, Prentice Hall, 592 pp.

Keshava, N., and Mustard, J.F., 2002. Spectral unmixing. IEEE Signal Processing Magazine, v. 19 (1), pp. 44-57.

Kruse, F.A., Kierein-Young, K.S., and Boardman, J.W., 1990. Mineral mapping at Cuprite, Nevada with a 63 channel imaging spectrometer. Photogrammetry Engineering and Remote Sensing, v. 56 (1), pp. 83-92.

Kurz, T., Gloaguen, R., Ebinger, C., Casey, M., and B., A., 2007. Deformation distribution and type in the Main Ethiopian Rift (MER): A remote sensing study. Journal of African Earth Sciences, v. 48 (2-3), pp. 100-114.

Leverington, D.W., 2010. Discrimination of sedimentary lithologies using Hyperion and Landsat Thematic Mapper data: a case study at Melville Island, Canadian High Arctic. International Journal of Remote Sensing, v. 31 (1), pp. 233 - 260.

Lim, M., Petley, D.N., Rosser, N.J., Allison, R.J., and Long, A.J., 2005. Combined digital photogrammetry and time-of-flight laser scanning for monitoring cliff evolution. The Photogrammetric Record, v. 20 (110), pp. 109-129.

Luhmann, T., Robson, S., Kyle, S., and Hartley, I., 2006. Close range photogrammetry: principles, techniques and applications. Dunbeath, Whittles Publ., 510 pp.

McCaffrey, K.J.W., Jones, R.R., Holdsworth, R.E., Wilson, R.W., Clegg, P., Imber, J., Hollman, N., and Trinks, I., 2005. Unlocking the spatial dimension: digital technologies and the future of geoscience fieldwork. Journal of the Geological Society, London, v. 162 (6), pp. 927-938.

Milan, D., 2009. Terrestrial laser scan-derived topographic and roughness data for hydraulic modelling of gravel-bed rivers. In: Heritage, G., and Large, A., (eds.), Laser scanning for the environmental sciences. Chichester, Wiley-Blackwell, pp. 133-146.

Nicodemus, F.E., Richmond, J.C., Hsia, J.J., Ginsberg, I.W., and Limperis, T., 1977. Geometrical Considerations and Nomenclature for Reflectance. National Bureau of Standards, US Department of Commerce, Washington, D.C. URL: http://physics.nist.gov/Divisions/Div844/facilities/specphoto/pdf/geoConsid.pdf

Olariu, M.I., Ferguson, J.F., Aiken, C.L.V., and Xu, X., 2008. Outcrop fracture characterization using terrestrial laser scanners: Deep-water Jackfork sandstone at Big Rock Quarry, Arkansas. Geosphere, v. 4 (1), pp. 247-259.

Phelps, R.M., Kerans, C., Scott, S.Z., Janson, X., and Bellian, J.A., 2008. Three-dimensional modelling and sequence stratigraphy of a carbonate ramp-to-shelf transition, Permian Upper San Andres Formation. Sedimentology, v. 55 (6), pp. 1777-1813.

Pringle, J.K., Howell, J.A., Hodgetts, D., Westerman, A.R., and Hodgson, D.M., 2006. Virtual outcrop models of petroleum reservoir analogues: a review of the current state-of-the-art. first break, v. 24, pp. 33-42.

Richter, R., 1998. Correction of satellite imagery over mountainous terrain. Applied Optics, v. 37 (18), pp. 4004−4015.

Rowlands, K.A., Jones, L.D., and Whitworth, M., 2003. Landslide Laser Scanning: a new look at an old problem. Quarterly Journal of Engineering Geology and Hydrogeology, v. 36 (2), pp. 155-157.

Schaepman-Strub, G., Schaepman, M.E., Painter, T.H., Dangel, S., and Martonchik, J.V., 2006. Reflectance quantities in optical remote sensing - definitions and case studies. Remote Sensing of Environment, v. 103 (1), pp. 27-42.

Short, N.M., and Blair, R.W., (eds.), 1986. Geomorphology from Space. Washington, DC, NASA SP-486 US Govt Printing Office, available at: http://disc.sci.gsfc.nasa.gov/geomorphology (accessed October 2010).

Slob, S., and Hack, R., 2004. 3D terrestrial laser scanning as a new field measurement and monitoring technique. In: Hack R., Azzam R., and Charlier R., (eds.), Engineering geology for infrastructure planning in Europe: A European perspective, 104, Lecture Notes in Earth Sciences. Heidelberg, Springer-Verlag, pp. 179-189.

Thomas, G.E., and Stamnes, K., 2002. Radiative transfer in the atmosphere and ocean. Cambridge, Cambridge University Press, 517 pp.

van der Meer, F.D., 2004. Analysis of spectral absorption features in hyperspectral imagery. International Journal of Applied Earth Observation and Geoinformation, v. 5 (1), pp. 55-68.

van der Werff, H., van der Meijde, M., Jansma, F., van der Meer, F.D., and Groothuis, G.J., 2008. A spatial-spectral approach for visualization of vegetation stress resulting from pipeline leakage. Sensors v. 8 (6), pp. 3733-3743, doi: 10.3390/s8063733.

Wehr, A., and Lohr, U., 1999. Airborne laser scanning - an introduction and overview. ISPRS Journal of Photogrammetry and Remote Sensing, v. 54 (2-3), pp. 68-82.

Windeler, D.S., and Lyon, R.J.P., 1991. Discriminating dolomitization of marble in the Ludwig Skarn near Yerington, Nevada using high-resolution airborne infrared imagery. Photogrammetric Engineering and Remote Sensing, v. 57 (9), pp. 1171-1177.

www1, 2010. JHU spectral library directed by John W. Salisbury. http://speclib.jpl.nasa.gov/documents/jhu_desc (accessed: September 2010)

www2, 2010. Chemical Education Digital Library. www.chemeddl.org/labs/avisualdatabase/index.php?molecule=10&sort=name&kind=all&molecule2=-1&sort2=name (accessed: September 2010)